Electronic Supplementary Information (ESI) for

Preferential Horizontal Growth of Tungsten Sulfide on Carbon and Insight into Active Sulfur Site for the Hydrogen Evolution Reaction

Bora Seo,[a,‡] Gwan Yeong Jung,[b,‡] Jae Hyung Kim,[b] Tae Joo Shin,[c] Hu Young Jeong,[c] Sang Kyu Kwak,[b] and Sang Hoon Joo*[a,b]*

[a]Department of Chemistry, and [b]School of Energy and Chemical Engineering, and [c]UNIST Central Research Facilities (UCRF), Ulsan National Institute of Science and Technology (UNIST), 50 UNIST-gil, Ulsan 44919, Republic of Korea.

[‡]These authors contributed equally to this work.

*E-mail: shjoo@unist.ac.kr (S.H.J.); skkwak@unist.ac.kr (S.K.K.)

Table of Contents

1. Supplementary Tables S1–S7 and Figs. S1–S10

Table S1 Contents (wt.%) of W, S, and C in WS_x@OMC, determined by quantitative EDS analysis.[a]

Sample	*Nominal loading* [b]	*W*	*S* [c]	*C*
2% WS_x@OMC	2	1.1 ± 0.3	6.0 ± 1.4	92.9 ± 1.2
5% WS_x@OMC	5	2.7 ± 1.0	6.9 ± 0.9	90.4 ± 1.6
10% WS_x@OMC	10	6.2 ± 0.7	5.7 ± 0.7	88.1 ± 1.0
15% WS_x@OMC	15	8.1 ± 0.9	6.1 ± 1.2	85.8 ± 2.0
20% WS_x@OMC	20	12.0 ± 2.5	5.5 ± 0.7	82.5 ± 2.7

[a] The contents were determined by averaging seven quantitative EDS results measured on different sites.

[b] The nominal loading was determined by the quantity of PTA precursor used in the synthesis.

[c] S species can exist as WS_x and S–C.

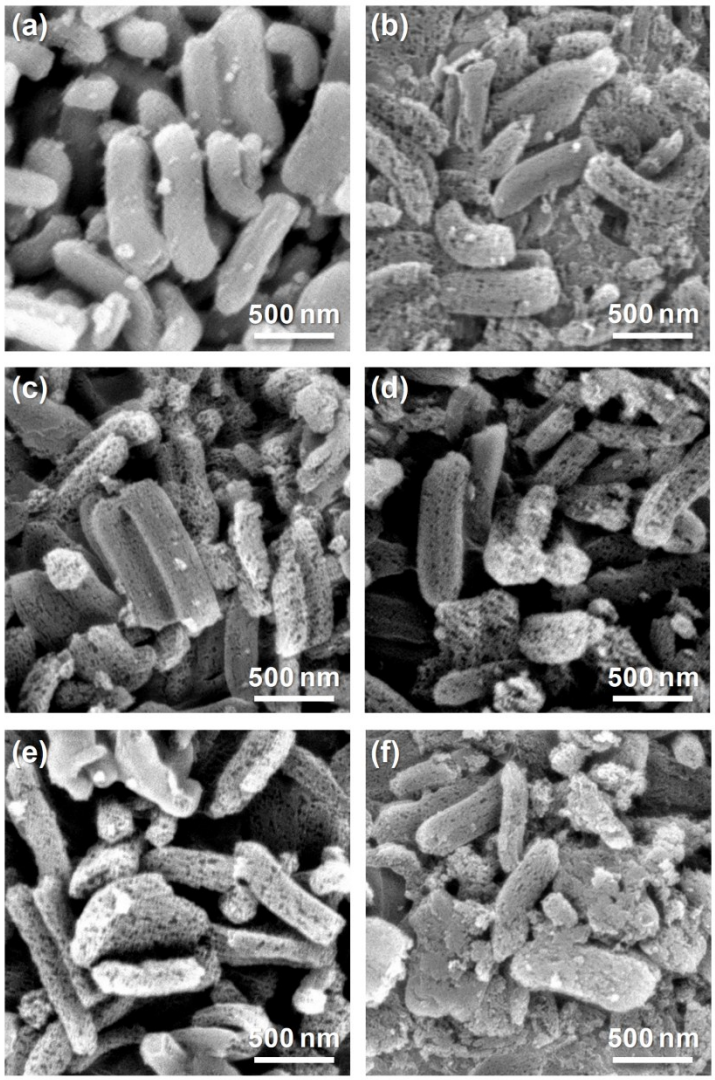

Fig. S1 SEM images of (a) SBA-15, (b) 2% WS_x@OMC, (c) 5% WS_x@OMC, (d) 10% WS_x@OMC, (e) 15% WS_x@OMC, and (f) 20% WS_x@OMC.

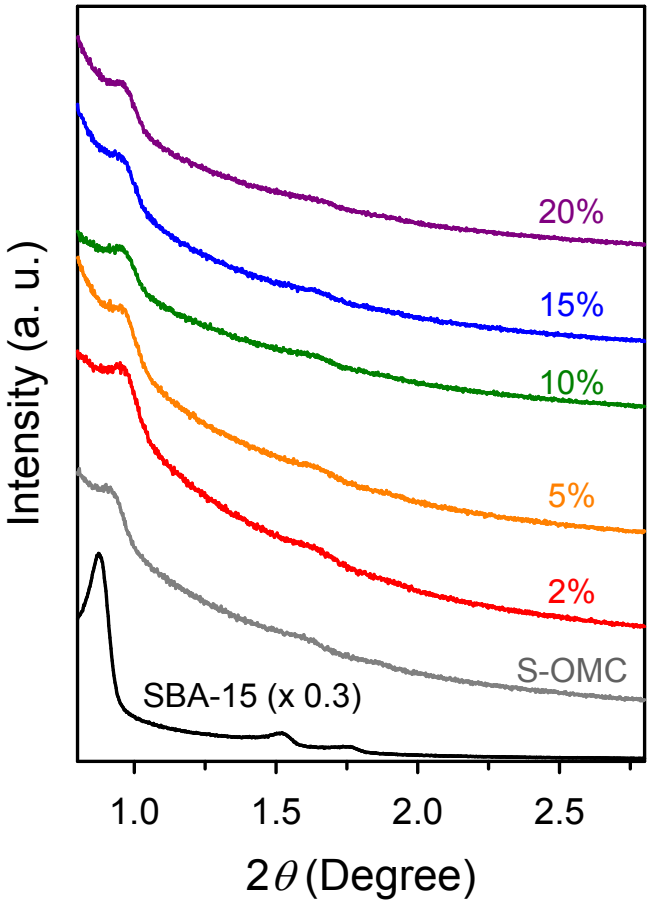

Fig. S2 Small-angle XRD patterns of SBA-15, S-OMC, and WS_x@OMCs.

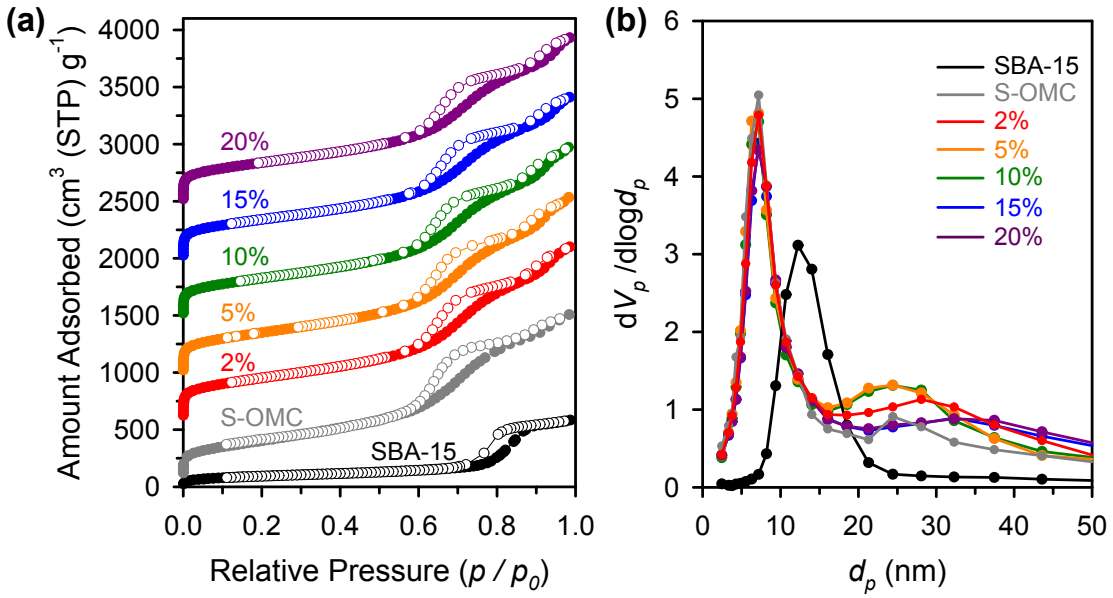

Fig. S3 (a) Nitrogen adsorption-desorption isotherms of SBA-15, S-OMC, and WS_x@OMCs. Filled circles and empty circles represent adsorption and desorption branches of the isotherms, respectively. The isotherms of S-OMC, 2 wt.%, 5 wt.%, 10 wt.%, 15 wt.%, and 20 wt.% WS_x@OMC were offset by 100, 600, 1000, 1500, 2000, and 2500 $cm^3\ g^{-1}$, respectively, for clarity. (b) The BJH pore size distributions of SBA-15, S-OMC, and WS_x@OMCs obtained from the adsorption branches of their isotherms.

Table S2 BET surface areas, total pore volumes, and pore sizes obtained from nitrogen adsorption–desorption analysis.

Sample	BET surface area [a] ($m^2\ g^{-1}$)	Pore volume [b] ($cm^3\ g^{-1}$)	Pore size [c] (nm)
SBA-15	337	0.90	12.2
OMC@SBA-15	464	0.52	7.2–10.7
S-OMC	1112	2.18	7.2, 24.4
2% WS_x@OMC	1265	2.32	7.2, 28.1
2% WS_x@OMC_20 h	1243	2.28	7.2, 32.3
5% WS_x@OMC	1259	2.37	7.2, 24.4
10% WS_x@OMC	1172	2.28	7.2, 24.4
15% WS_x@OMC	1217	2.18	7.2, 32.3
20% WS_x@OMC	1210	2.21	7.2, 32.3

[a] BET surface area was obtained in the relative pressure range of 0.05–0.2.

[b] Pore volume was determined at the relative pressure of 0.98–0.99.

[c] Pore size was determined by using the BJH method from the adsorption branch of the isotherms.

Table S3 Basal plane crystallite sizes of WS_2 nanoplates determined by the TEM images.

Sample	Basal plane size [a] (nm)
2% WS_x@OMC	- [b]
2% WS_x@OMC_20 h	7.1 ± 4.5
5% WS_x@OMC	4.4 ± 2.1
10% WS_x@OMC	4.7 ± 2.5
15% WS_x@OMC	4.1 ± 2.0
20% WS_x@OMC	4.6 ± 2.6

[a] Basal plane sizes were measured on the particles in TEM images. The values were obtained by averaging the measured sizes of at least one hundred of particles.

[b] In this sample, most of WS_x exist in the form of subnanometer-sized clusters.

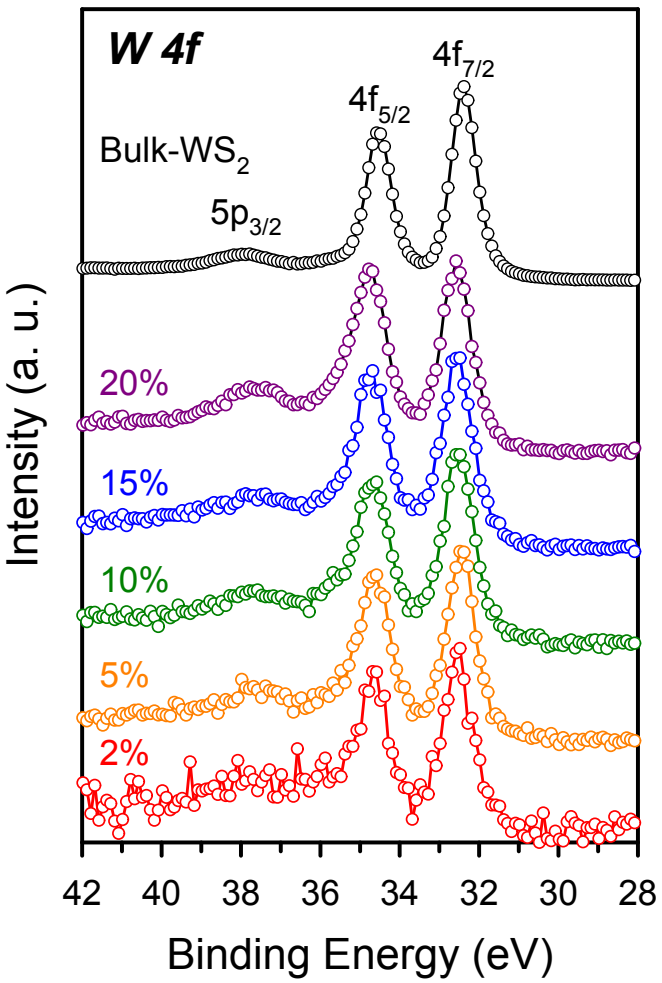

Fig. S4 W 4f XPS spectra for bulk-WS_2 and WS_x@OMCs.

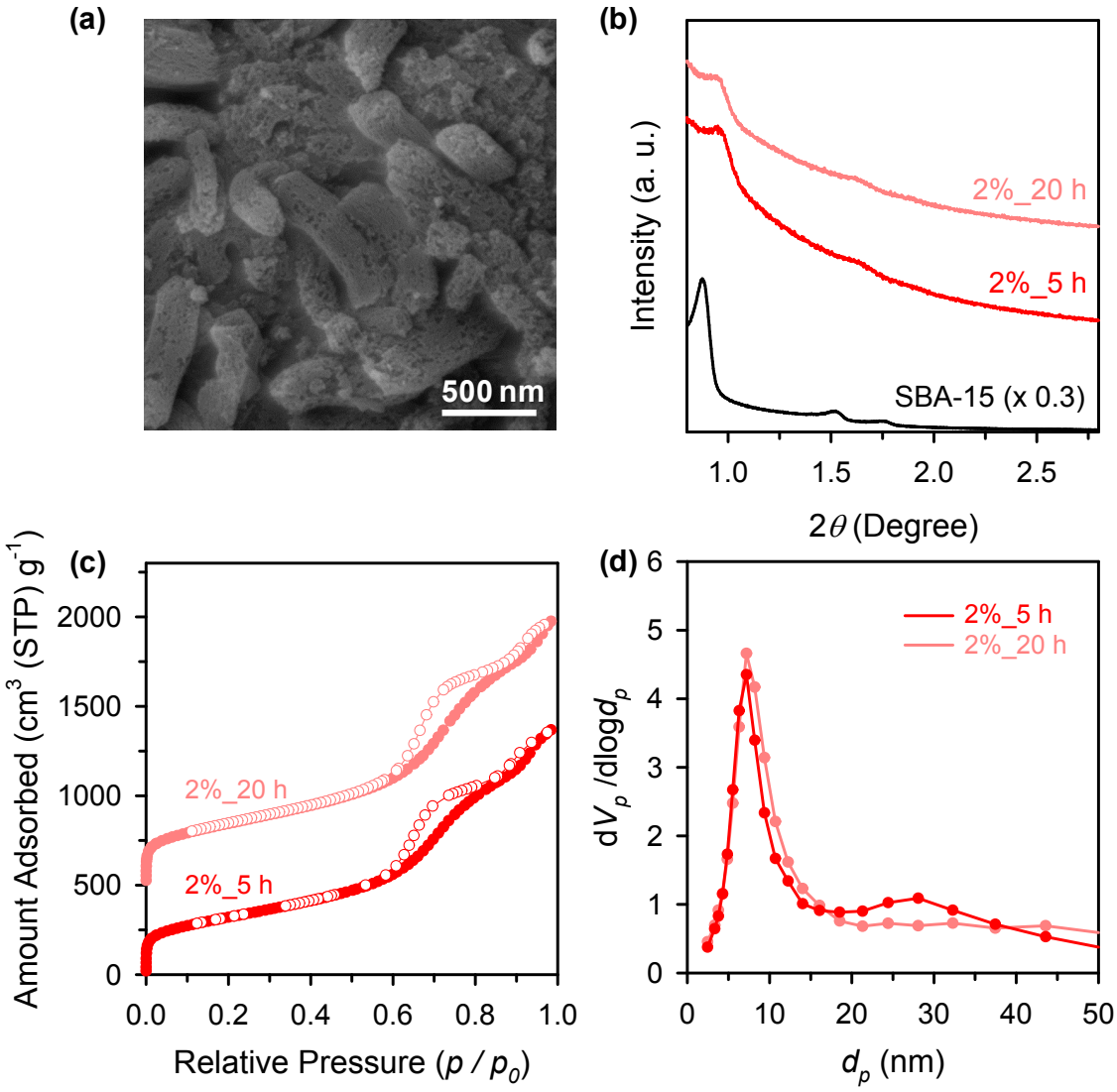

Fig. S5 (a) SEM image of 2% WS_x@OMC prepared with a sulfidation time of 20 h. (b) Small-angle XRD patterns for SBA-15 and 2% WS_x@OMCs prepared with different sulfidation time of 5 h and 20 h. (c) Nitrogen adsorption-desorption isotherms for 2% WS_x@OMCs prepared with different sulfidation time. Filled circles and empty circles represent adsorption and desorption branches of the isotherms, respectively. The isotherms of the 20 h sample was offset by 500 cm^3 g^{-1}, for clarity. (d) The BJH pore size distributions obtained from the adsorption branches of the isotherms.

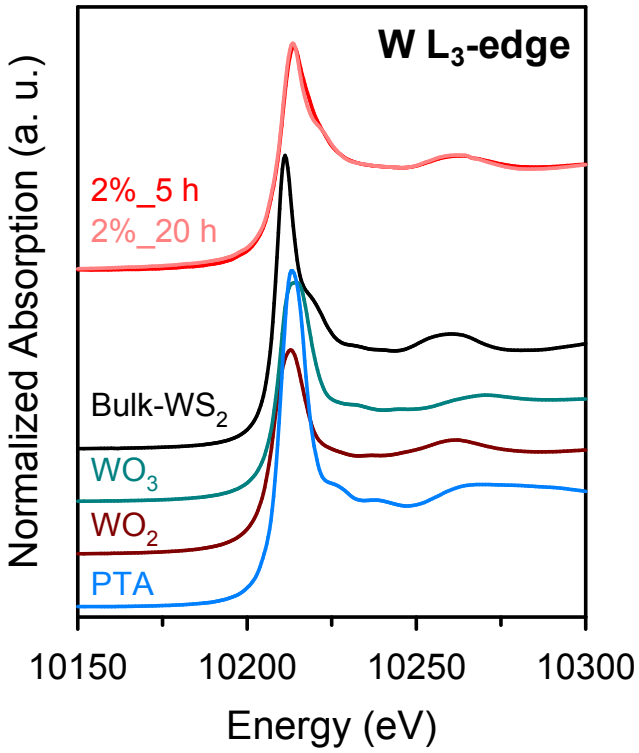

Fig. S6 W L_3-edge XANES spectra of 2% WS_x@OMCs prepared with different sulfidation times of 5 h and 20 h, displayed with reference samples.

Table S4 Structural parameters derived from fitted EXAFS spectra for bulk-WS_2 and 2% WS_x@OMC samples prepared with different sulfidation times of 5 h and 20 h.

Sample	Shell	CN	R (Å)	ΔE_0	σ^2 ($\times 10^{-3}$ Å^{-2})	R factor (%)
Bulk-WS_2	W-S_1	6	2.394 (8)	6.0	1.9 (9)	0.96
	W-W	6	3.161 (16)	6.4	2.4 (9)	
	W-S_2	6	3.949 (25)	6.0	4.4 (30)	
2%_20 h	W-S_1	4.8 ± 0.5	2.399 (5)	7.1	1.9 [a]	1.31
	W-W [b]	3.8 ± 0.6	3.151 (12)	5.3	2.4	
	W-S_2	3.8 ± 0.6	3.952 (22)	7.1	4.4	
2%_5 h	W-S_1	3.8 ± 0.4	2.408 (8)	8.7	1.9	3.13
	W-W	2.6 ± 0.6	3.129 (23)	2.6	2.4	
	W-S_2	2.6 ± 0.6	3.996 (44)	8.7	4.4	

[a] Debye-Waller parameter (σ^2) was fixed to the same value in the same type of bond.

[b] Bonds of W–W and W–S_2 were set to have the same CN.

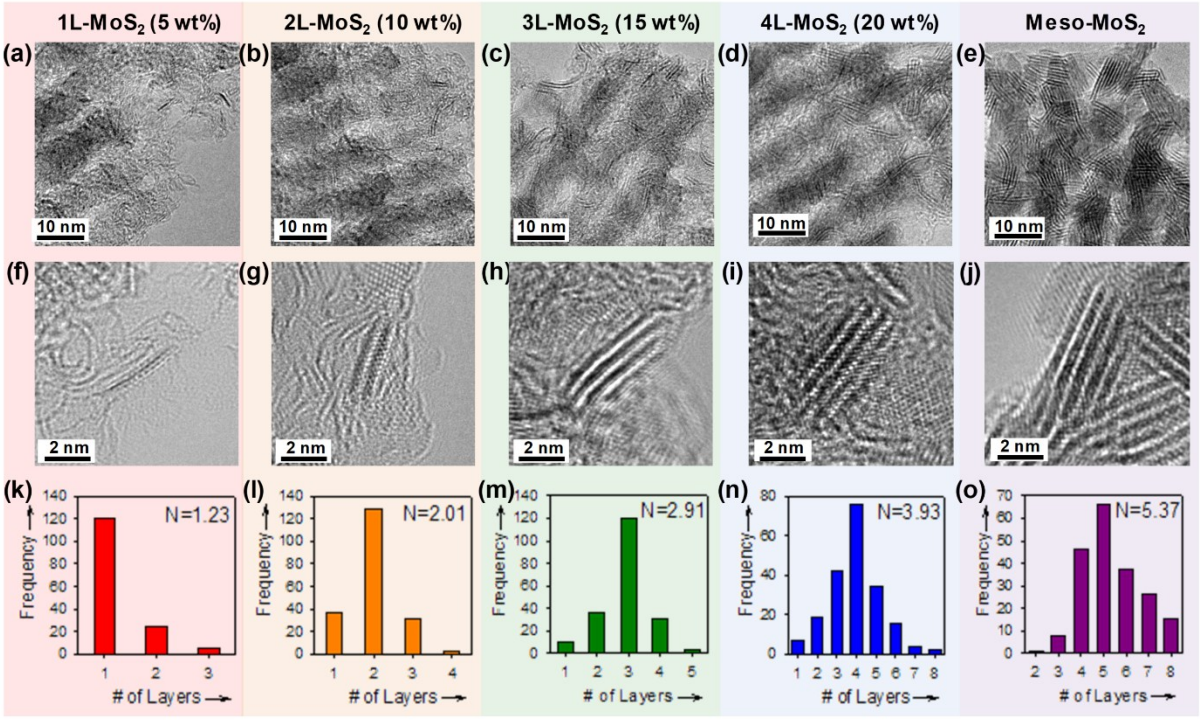

Fig. S7 TEM images of (a) 1L-MoS_2@OMC, (b) 2L-MoS_2@OMC, (c) 3L-MoS_2@OMC, (d) 4L-MoS_2@OMC, and (e) Meso-MoS_2. Corresponding AR-TEM images (f–j) and histograms for layer number distribution (k–o). The average number of MoS_2 layers is denoted as 'N' in (k–o). The figure is modified from our previous work.[S1]

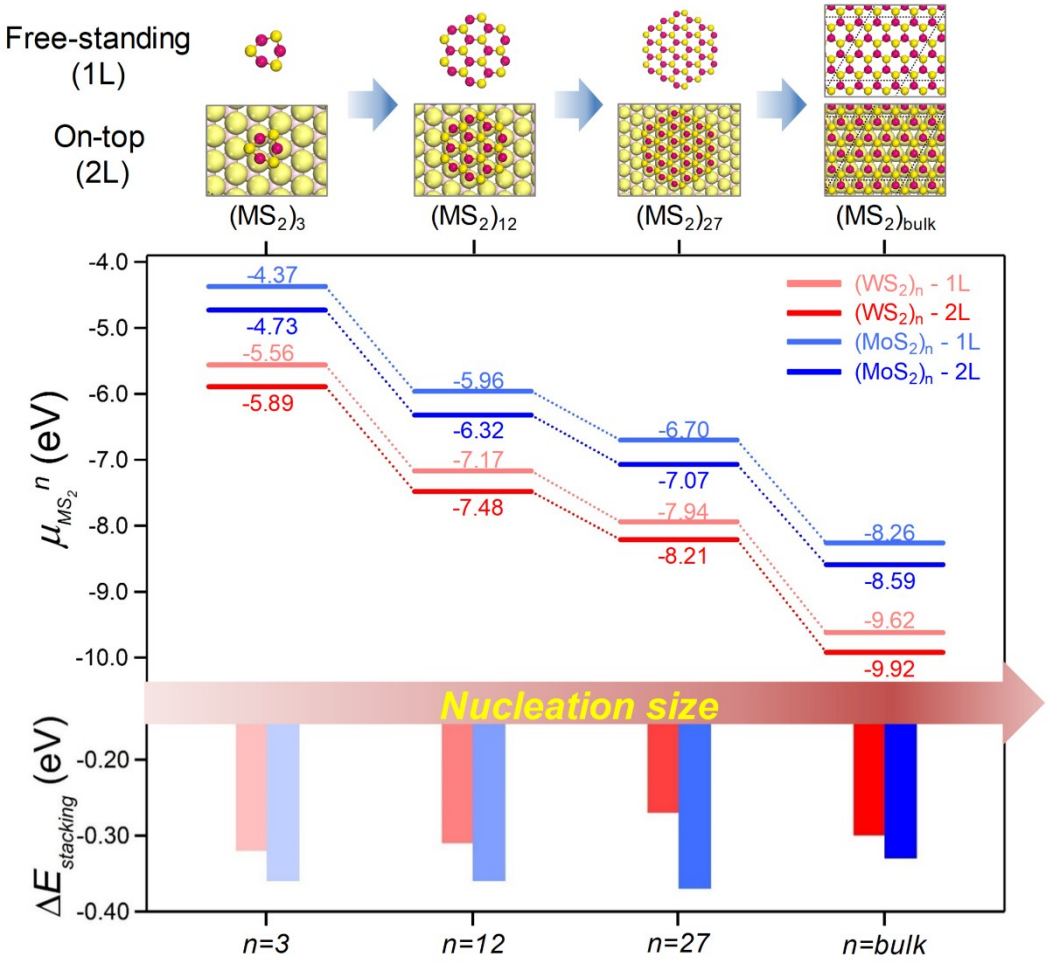

Fig. S8 Top view of $(MS_2)_n$ cluster models (n = 3, 12, 27, and bulk state, M = W, Mo) and the energy diagram for the unit potential energy ($\mu^n_{MS_2}$). The M and S atoms are represented by red and yellow spheres, respectively. In the 'on-top' (2L) model, the M and S atoms in the bottom layer are presented as light red and light yellow spheres, respectively.

Table S5 Unit potential energies (eV, $\mu^{n}_{MS_2}$) and stacking energies ($\Delta E_{stacking}$) of MS_2 cluster models (M = W, Mo).

		$(MS_2)_3$	$(MS_2)_{12}$	$(MS_2)_{27}$	$(MS_2)_{bulk}$
WS_2	Free-standing **(1L)** [a]	-5.56	-7.17	-7.94	-9.62
	On-top **(2L)** [b]	-5.89	-7.48	-8.21	-9.92
	Stacking energy ($\Delta E_{stacking}$)	-0.33	-0.31	-0.27	-0.30
MoS_2	Free-standing **(1L)** [a]	-4.37	-5.96	-6.70	-8.26
	On-top **(2L)** [b]	-4.73	-6.32	-7.07	-8.59
	Stacking energy ($\Delta E_{stacking}$)	-0.36	-0.36	-0.37	-0.33

[a] Free-standing (1L) denotes the $\mu^{n}_{MS_2}$ of free-standing single layer MS_2 cluster model.

[b] On-top (2L) denotes the $\mu^{n}_{MS_2}$ of on-top double layer MS_2 cluster model.

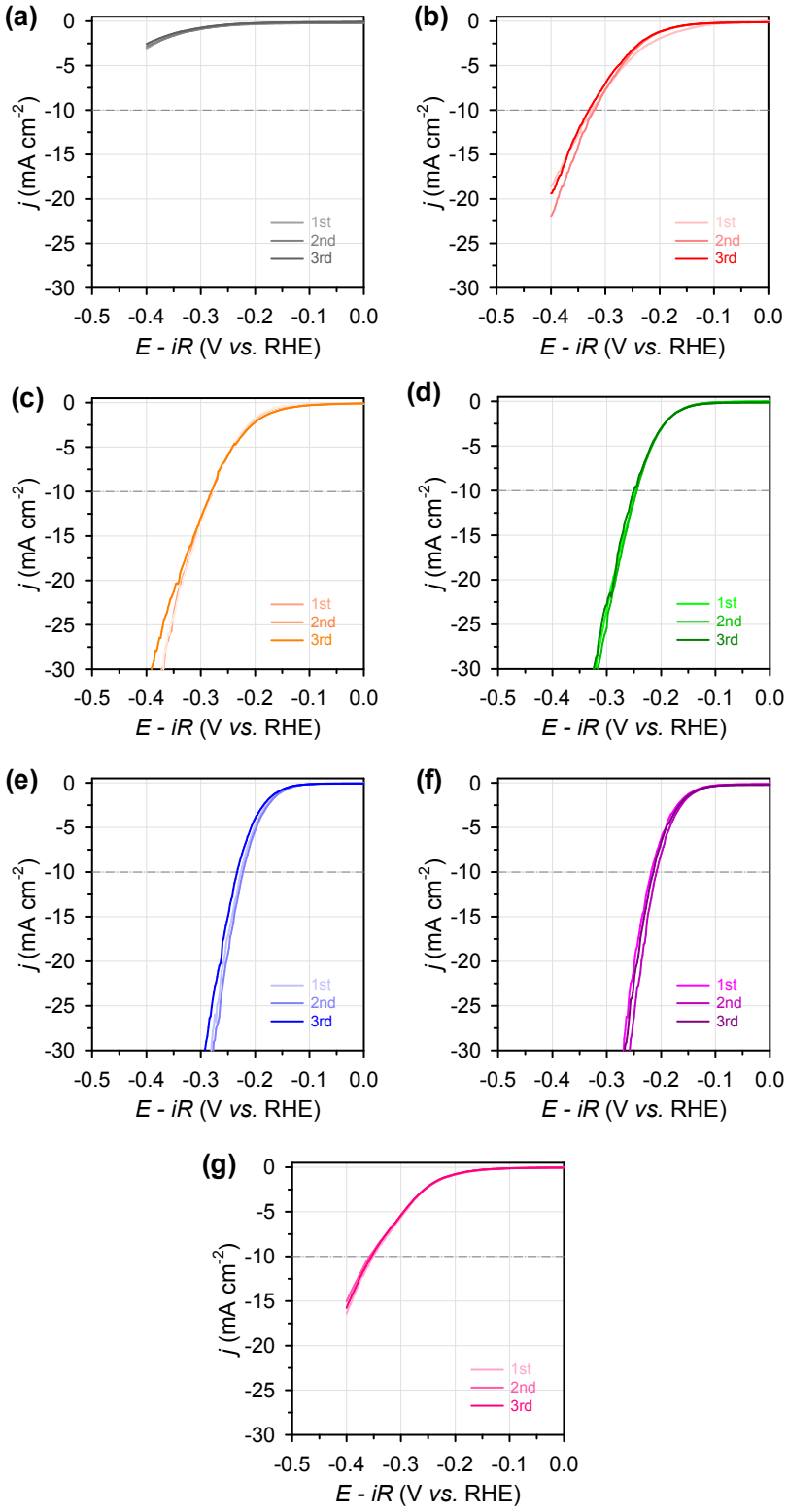

Fig. S9 Raw data for LSV curves of (a) S-OMC, (b) 2% WS_x@OMC, (c) 5% WS_x@OMC, (d) 10% WS_x@OMC, (e) 15% WS_x@OMC, (f) 20% WS_x@OMC, and (g) 2% WS_x@OMC_20 h.

Table S6 HER activities of WS_x@OMC nanostructures in terms of overpotential at −10 mA cm^{-2}, Tafel slope, and exchange current density.

Sample	Overpotential at 10 mA cm^{-2} (V)	Tafel slope [a] ($mV\ dec^{-1}$)	Exchange current density [b] ($A\ cm^{-2}$)
2% WS_x@OMC	325	129	4.14×10^{-5}
2% WS_x@OMC_20 h	354	117	1.55×10^{-5}
5% WS_x@OMC	279	95	1.50×10^{-5}
10% WS_x@OMC	247	72	5.02×10^{-6}
15% WS_x@OMC	226	68	5.30×10^{-6}
20% WS_x@OMC	213	74	1.34×10^{-5}

[a,b] The Tafel slopes and exchange current densities were derived from the linear portion of the corresponding Tafel plots.

Table S7 Comparison of loadings, overpotentials, and Tafel slopes of WS_x-based electrocatalysts for HER.

Catalysts	Loading (μg cm^{-2})	Overpotential at 10 mA cm^{-2} (V)	Tafel slope (mV dec^{-1})	Ref.
2% WS_x@OMC	230 (~4.6 μg for WS_x)	0.325	129	This work
20% WS_x@OMC	230 (~46 μg for WS_x)	0.213	74	
1T-WS_2	-	0.365	85	S2
$CoWS_x$	-	0.373	78	S3
WS_2-rGO	400	0.260	58	S4
WS_2 nanoflakes	1000	0.350	200	S5
WS_2/CC	14 for WS_2	0.214	68	S6
Metallic WS_2 nanosheets	1000	0.140	70	S7
WS_2 nanoribbons	-	0.240	68	S8
WS_2 nanoflakes	350	0.158	48	S9
G-WS_2	100	0.306	67	S10
1T-WS_2 nanosheets	6.5	0.230	55	S11
WS_2 quantum dots	-	0.330	70	S12
3D WS_2 @P,N,O-graphene	113	0.125	52.7	S13
WS_2-rGO	562	0.170	52	S14
WS_2 nanosheets	-	0.278	120	S15
WS_2 nanorattle	350	0.192	68	S16
WS_2/WS_3 film	-	0.494	43.7	S17

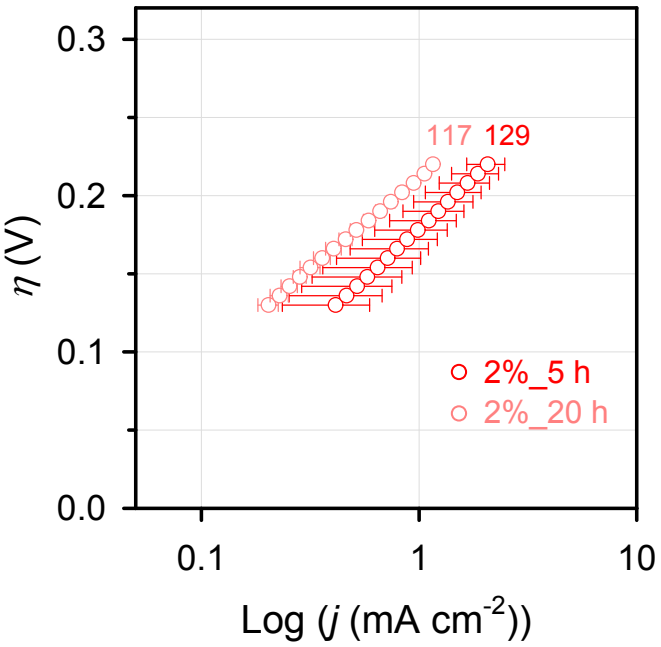

Fig. S10 Tafel plots for 2% WS_x@OMCs prepared with different sulfidation times of 5 h and 20 h. Considering the error ranges, the Tafel slopes are similar to each other.

2. References for ESI

S1 B. Seo, G. Y. Jung, Y. J. Sa, H. Y. Jeong, J. Y. Cheon, J. H. Lee, H. Y. Kim, J. C. Kim, H. S. Shin, S. K. Kwak and S. H. Joo, *ACS Nano*, 2015, **9**, 3728–3739.

S2 D. Voiry, H. Yamaguchi, J. Li, R. Silva, D. C. B. Alves, T. Fujita, M. Chen, T. Asefa, V. B. Shenoy, G. Eda and M. Chhowalla, *Nat. Mater.*, 2013, **12**, 850–855.

S3 P. D. Tran, S. Y. Chiam, P. P. Boix, Y. Ren, S. S. Pramana, J. Fize, V. Artero and F. Barber, *Energy Environ. Sci.*, 2013, **6**, 2452–2459.

S4 J. Yang, D. Yoiry, S. J. Ahn, D. Kang, A. Y. Kim, M. Chhowalla and H. S. Shin, *Angew. Chem. Int. Ed.*, 2013, **52**, 13751–13754.

S5 C. L. Choi, J. Feng, Y. Li, J. Wu, A. Zak, R. Tenne and H. Dai, *Nano Res.*, 2013, **6**, 921–928.

S6 T.-Y. Chen, Y.-H. Chang, C.-L. Hsu, K.-H. Wei, C.-Y. Chiang and L.-J. Li, *Int. J. Hydrogen Energy*, 2013, **38**, 12302–12309.

S7 M. A. Lukowski, A. S. Daniel, C. R. English, F. Meng, A. Forticaux, R. J. Hamers and S. Jin, *Energy Environ. Sci.*, 2014, **7**, 2608–2613.

S8 J. Lin, Z. Peng, G. Wang, D. Zakhidov, E. Larios, M. J. Yacaman and J. M. Tour, *Adv. Energy Mater.*, 2014, **4**, 1301875.

S9 L. Cheng, W. Huang, Q. Gong, C. Liu, Z. Liu, Y. Li and H. Dai, *Angew. Chem. Int. Ed.*, 2014, **53**, 7860–7863.

S10 Z. Pu, Q. Liu, A. M. Asiri, A. Y. Obaid and X. Sun, *Electrochim. Acta*, 2014, **134**, 8–12.

S11 A. Ambrosi, Z. Sofer and M. Pumera, *Chem. Commun.*, 2015, **51**, 8450–8453.

S12 S. Xu, D. Li and P. Wu, *Adv. Funct. Mater.*, 2015, **25**, 1127–1136.

S13 J. Duan, S. Chen, B. A. Chambers, G. G. Andersson and S. Z. Qiao, *Adv. Mater.*, 2015, **27**, 4234–4241.

S14 J. Zhang, Q. Wang, L. Wang, X. Li and W. Huang, *Nanoscale*, 2015, **7**, 10391–10397.

S15 T. P. Nguyen, S. Choi, J.-M. Jeon, K. C. Kwon, H. W. Jang and S. Y. Kim, *J. Phys. Chem. C*, 2016, **120**, 3929–3935.

S16 Y. Wen, Y. Xia and S. Zhang, *J. Power Sources*, 2016, **307**, 593–598.

S17 S. M. Tan and M. Pumera, *ACS Appl. Mater. Inter.*, 2016, **8**, 3948–3957.